

BOOK: PRCs in Neuroscience; Theory, Experiment and Analysis***Section CB: Prediction of Network States; Experiment***

Title: Understanding activity in electrically coupled networks using PRCs and the theory of weakly coupled oscillators.

Authors: T.J. Lewis⁺ and F.K. Skinner^{*}

Abstract

In this chapter, we describe in detail how phase-locking in electrically coupled networks of spiking neurons can be understood using the framework of PRCs and weak coupling theory. We provide the necessary mathematical background and biological context to allow the reader to acquire an understanding of the network dynamics. We present the work using neuronal representations that include general integrate-and-fire and conductance-based models as well as spatially distributed, compartmental models.

1. Introduction

Neurons communicate with each other by electrical and chemical synapses. Chemical communication involves the release of neurotransmitters from presynaptic neurons into a synaptic cleft that separates presynaptic and postsynaptic neurons. Electrical communication on the other hand occurs by direct intercellular channels between presynaptic and postsynaptic neurons. These intercellular channels consist of two hemichannels called connexons, and each hemichannel is composed of six specialized protein molecules called connexins. A gap junction is a cluster of these channels (See Meier & Dermietzel, 2006 for more detail). Several types of connexin gap junction proteins are expressed in neurons, but connexin36 is expressed exclusively in neurons. In particular, connexin36 mediates the extensive electrical coupling between many cortical inhibitory neurons (Connors & Long, 2004; Galarreta & Hestrin, 2001; Söhl et al., 2005). Although chemical synapses are more common in neural systems and have been studied more extensively, electrical synapses are more advanced from an evolutionary

⁺ **Shared First Authorship**, TJL, Department of Mathematics, University of California, Davis

^{*} **Shared First Authorship**, FKS, Toronto Western Research Institute, University Health Network and University of Toronto

perspective (Bennett, 2000) and provide connection characteristics that are different from those of chemical synapses. Specifically, they provide fast, bidirectional coupling and include coupling of subthreshold voltages. Functionally, they are thought to play a role in synchronization of neuronal activity, but the details are far from clear.

The goal for this chapter is to discuss how synchronization patterns depend on a neuron's intrinsic properties and the electrical coupling. Specifically, we will show how phase response curves in conjunction with the theory of weakly coupled oscillators (see introductory Chapter X) can provide important insight into this issue.

1.1 Basic model and actions of gap junction coupling

Gap junctions can sometimes exhibit rectification and voltage-gating (Hormuzdi et al., 2004), and models of electrical coupling can involve considerable complexity (e.g. Vogel & Weingart, 2002). However, gap junctions largely act like electrical resistors (Bennett, 1977). Therefore, we will only consider mathematical models of gap junctions as simple ohmic resistors. Specifically, the basic current balance equation that we will use for a pair of electrically coupled neurons is:

$$C \frac{dV_j}{d\tilde{t}} = -I_{ionic,j} + I_{app,j} + g_{gap}(V_k - V_j), \quad \dots \text{ (eq: current),}$$

where \tilde{t} is time, C is the membrane capacitance, V_j is the membrane potential of the cell j , $I_{app,j}$ is a constant applied current (injected DC current) to cell j , and $I_{ionic,j}$ is the ionic current of cell j . The electrical coupling current flowing from cell k into j is modeled as $I_{gap,j:k} = g_{gap}(V_k - V_j)$, where g_{gap} is the gap junction coupling conductance.

It can be seen from equation (eq:current) that the electrical coupling current between cells flows down the electrical gradient and tends to bring the cells' membrane potentials closer together. As such, we intuitively expect electrical coupling to synchronize activity. This naturally synchronizing action of gap junctions (due to their rapid, bidirectional natures) has been discussed in several reviews (Bennett & Zukin, 2004; Connors & Long, 2004; Galarreta & Hestrin, 2001). However, modeling work has shown that electrical coupling can support both synchronous and asynchronous activities (Bem et al., 2005; Chow & Kopell, 2000; Cymbalyuk et al., 1994; Lewis & Rinzel, 2003; Sherman & Rinzel, 1992). Furthermore, stable anti-phase activity has specifically been found in many conductance-based models of

electrically coupled pairs of cortical inhibitory interneurons (Di Garbo et al., 2005; Lewis & Rinzel, 2004; Mancilla et al., 2007; Nomura et al., 2003; Pfeuty et al., 2003; Skinner et al., 1999). Gap junctions in conjunction with the cell membrane act as low pass filters, and therefore a “presynaptic” spike gives rises to an attenuated and delayed voltage response in the “postsynaptic” cell. Measured postsynaptic responses (spikelets) vary in size and can include both depolarizing and hyperpolarizing components. This depends on the details of the spike shape, such as spike width and afterhyperpolarization, as well as where the gap junctions are located and where postsynaptic responses are measured. Moreover, spike frequency would be expected to affect the resulting network dynamics. These aspects make it difficult to intuit the output from electrically coupled networks,

How can we more fully understand the actions of gap junction coupling? Only a limited amount of information and mechanistic understandings can be obtained using direct numerical simulations. We therefore turn to phase response curves and the theory of weakly coupled oscillators (Kuramoto, 1984).

1.2 PRCs and the theory of weakly coupled oscillators

As described in the introductory Chapter X, the phase response curve (PRC), or the phase resetting curve describes whether a perturbation advances or delays the phase of a periodically firing neuron.¹ PRCs have been used to predict phase-locking behaviors for periodic, pulsatile stimuli (Glass & Mackey, 1988; Rinzel & Ermentrout, 1998) and for cell pairs connected by fast, pulsatile chemical synapses (see Chapter XX). PRCs can also be used to predict phase-locking in networks of oscillators with general coupling, including electrical coupling, provided that the coupling is sufficiently weak. This latter case employs the theory of weak coupling (Kuramoto, 1984). The PRC used in this theory measures the response to brief, small current pulses² and is often referred to as the infinitesimal PRC (iPRC).

PRCs are often divided into two classifications: Type I PRCs are non-negative, meaning that spikes can only be advanced with perturbations, and type II PRCs are biphasic, usually with negative aspects at early phases and positive aspects at later phases (i.e., spikes can be advanced or delayed depending on the timing of the perturbation relative to the spike). Note that phase zero is typically defined as the peak of the spike at the soma, and we follow this definition in this chapter. Whether a neuron exhibits type I or

¹ These phase shifts are usually assessed by spike times.

² Theoretically, a delta-function current stimulus with small amplitude (in terms of total charge injected) is used to compute the iPRC. The iPRC can also be computed by linearizing the system about the limit cycle and solving the adjoint problem (see introductory Chapter X).

type II PRCs can be important because it has implications for synchrony in networks coupled with chemical synapses (e.g., see Crook et al. 1998b; Hansel et al., 1995), and this has been taken advantage of in examining how cholinergic neuromodulation might affect whether type I or type II PRC characteristics are present (Stiefel et al., 2009).

The basic mathematical equations for weakly coupled oscillator theory have been described in the introductory Chapter X and the same notation is followed in this chapter. When coupling between oscillators is sufficiently weak, the state of each oscillator can be captured by its relative phase, and the dynamics of a pair of identical cells connected by electrical coupling is governed by

$$\frac{d\psi_j}{dt} = \frac{1}{T} \int_0^T Z(\tilde{t}) g_{gap} \left(V_{LC}(\tilde{t} - (\psi_j - \psi_k)) - V_{LC}(\tilde{t}) \right) d\tilde{t} = g_{gap} H(-(\psi_j - \psi_k)), \quad \dots \text{ (eq: H)}$$

where ψ_j is the relative phase of the j^{th} cell, $V_{LC}(t)$ is the T -periodic membrane potential of the unperturbed (uncoupled) neurons, and $Z(t)$ is the iPRC of the neurons. The evolution of the phase difference between the cells, $\varphi = \psi_1 - \psi_2$, is described by the scalar differential equation

$$\frac{d\varphi}{dt} = g_{gap} (H(-\varphi) - H(\varphi)) = g_{gap} G(\varphi), \quad \dots \text{ (eq: G)}.$$

Phase differences φ^* with $G(\varphi^*) = 0$ are phase-locked states. A phase-locked state is stable if $G'(\varphi^*) < 0$ and unstable if $G'(\varphi^*) > 0$. Note that the coupling strength g_{gap} simply scales the G -function. It does not affect the existence or stability of the phase-locked states; it only affects how fast the system approaches or diverges from the phase-locked state and how robust the phase-locked states are to noise and heterogeneities (see introductory Chapter X for details). Note also that when the electrically coupled cells are identical, both the synchronous state $\varphi^* = 0, T$ and the anti-phase state $\varphi^* = T/2$ are phase-locked states, as can be seen by equation (eq: G). Furthermore, the stability of the anti-phase state is given by the sign of $G'(T/2) = -2 H'(T/2)$. These observations will be useful in our analysis.

The form of the G -function relates the existence, stability and robustness of phase-locked states to the iPRC, Z , and the membrane potential, V_{LC} . Z and V_{LC} are strictly properties of the individual neurons, and they are relatively easy to obtain for model cells and for real cells. Thus, the theory of weak coupling provides a two step method to obtain insight into both the dynamical and biophysical mechanisms underlying phase-locking:

Step 1: Determine how the shapes of Z and V_{LC} affect phase-locking, i.e., study how the shapes of the functions Z and V_{LC} combine (according to the “convolution” integral in the phase equations (eq: H)) to influence the phase-locked states.

Step 2: Explore how the shape of Z and V_{LC} are altered by changes in frequency or individual membrane conductances or by the presence of neuromodulators (or effects of anesthetics, pharmacological agents, temperature, pH, and so on), i.e., if we understand how the shapes of Z and V_{LC} alter phase-locking, then the problem of ‘understanding how membrane conductances affect phase-locking’ is reduced to ‘understanding how they affect Z and V_{LC} .’ While this latter problem is still non-trivial, it is a much more manageable problem than the former one.

1.3 Chapter outline and limitations

In this chapter, we describe how phase response curves (PRCs) and weakly coupled oscillator theory can be used to understand activities produced by electrically coupled cells. For space reasons, we take a narrow focus, only considering *electrical coupling* between *pairs of spiking* neurons in cortical systems and related theoretical works.³ As such, important work on electrical coupling involving bursting cells, non-neuronal cells (such as glia), non-spiking cells and invertebrate systems are not included in this chapter. We examine mathematical models that include the basic features of spiking neurons and coupling dynamics. With simpler neuronal caricatures, more extensive analyses can be performed. In general, analyses provide a theoretical framework with which to understand the behavior of more complicated models and experimental preparations, as well as the *in situ* physiological system.

In what follows, we describe the work that has been done using mathematical models of electrically coupled neuronal networks and the insights into the mechanisms underlying synchronization patterns in these networks. We start by describing simple two-cell networks that do not include a biophysical description for the individual neuron and then continue with two-cell networks that do include a biophysical description and that consider gap junctions that are not located close to the cell body. Finally, we provide a short summary and discussion.

³ Chapter XXX extends the analysis presented in this chapter to larger networks and considers coupling through both chemical synapses and electrical synapses.

2. Single-Compartment Integrate-and-Fire Models for Electrically Coupled Cell-Pairs

In this section, we consider phase-locking of pairs of one-variable single-compartment integrate-and-fire neurons that are connected by electrical coupling. The dynamics of the cell-pairs are given by

$$C \frac{dV_j}{dt} = -I_{ionic}(V_j) + I_{app} + g_{gap}(V_k - V_j), \quad \dots \text{ (eq: gif).}$$

Note that the ionic current $I_{ionic}(V_j)$ depends only on the membrane potential of the cell. These dynamics are augmented by a fire-and-reset rule: When V_j reaches a threshold potential V_{th} , cell j fires a “spike” and V_j is reset to the potential V_{reset} .⁴ The suprathreshold portion of a spike is modeled as a delta-function. Each time a cell fires, $\tilde{\beta}\delta(t)$ is added to its membrane potential (Lewis & Rinzel, 2003; Pfeuty et al., 2003).

If $I_{app} \leq I_{ionic}(V_j)$ for $V_{reset} \leq V_j \leq V_{th}$, then the isolated cells eventually approach a stable resting potential and do not fire. If $I_{app} > I_{ionic}(V_j)$ for $V_{reset} \leq V_j \leq V_{th}$, then V_j increases monotonically from V_{reset} until it reaches the threshold potential V_{th} at which point the cell ‘fires’. V_j is then reset to V_{reset} , and the process is repeated. Thus, for sufficiently large applied current, integrate-and-fire cells display periodic oscillations. The frequency of the oscillations increases with I_{app} .

Electrically coupled cell-pairs that are modeled using standard leaky-integrate-and-fire (LIF) dynamics (i.e., without the delta-function spike) exhibit anti-phase only activity for all applied currents and coupling strengths.⁵ This highlights the fact that electrotonic effects of the spikes play an essential role in determining phase-locking patterns (Chow & Kopell, 2000; Lewis & Rinzel, 2003; Pfeuty et al., 2003), and therefore they must be included in any adequate model of electrically coupled cells. As mentioned above, we model the suprathreshold portion of a spike as a delta-function $\tilde{\beta}\delta(t)$.⁶ Thus, a spike in one cell will instantaneously increase the membrane potential of the other cell towards threshold by a fixed

⁴ These models could be augmented with refractory period and time-dependent thresholds.

⁵ In fact, it can be shown that, as $g_{gap} \rightarrow \infty$, any single-variable IF model will support only anti-phase activity, whereas any single-compartment conductance-based model will support only synchronous activity (Lewis, unpublished results).

⁶ For certain IF models such as QIF, the spike could also be modeled by tuning V_{th} , so that the membrane potential rises rapidly to a high level before being reset (as in Latham et al., 2000).

amount $g_{gap}\tilde{\beta}$. With this spike effect included, the LIF model can exhibit both synchrony and anti-phase (Figure 1).

Below, we consider leaky integrate-and-fire (LIF) and quadratic integrate-and-fire (QIF) dynamics as specific examples, but we also provide some results for general integrate-and-fire (GIF) dynamics, i.e., integrate-and-fire with any $I_{ionic}(V)$. Most of these results are presented in Lewis & Rinzel (2003) and Pfeuty et al. (2003). The results highlight the importance of the shape of the iPRC and the components of the membrane potential waveform.

2.1 LIF, QIF and GIF dynamics

LIF dynamics: For the leaky integrate-and-fire (LIF) model, the ionic current is described only by the leakage current

$$I_{ionic}(V) = g_m(V - V_r),$$

where V_r is the reversal potential of the leakage current, and g_m is the membrane leakage conductance of the cell. In non-dimensional form (see Appendix 1), the LIF model is

$$\frac{dv_j}{dt} = -v_j + I,$$

with a threshold potential of 1 and a reset potential 0. For $I > 1$, LIF cells fire periodically with a membrane potential waveform of

$$v_{LC}(t) = I(1 - e^{-t}) + \beta \delta(t - T), \quad t \in [0, T]$$

and a period of oscillation

$$T = \ln\left(\frac{I - v_{reset}}{I - v_{th}}\right) = \ln\left(\frac{I}{I - 1}\right).$$

The infinitesimal phase-response curve $Z(t)$ for the LIF model (Hansel et al., 1995; Neltner et al., 2000) is

$$Z(t) = \begin{cases} \frac{1}{I} \exp(t), & 0 < t < T \\ 0, & t = 0, T \end{cases}.$$

Several ways to derive $Z(t)$ for LIF cells are covered in the appendix of Lewis & Rinzel, 2003.

QIF dynamics: For the quadratic integrate-and-fire (QIF) model, the ionic current is

$$I_{ionic}(V) = g_m \frac{(V_T - V)(V - V_R)}{(V_T - V_R)},$$

where V_R and V_T are the resting potential and “resting threshold” potential⁷ of the neuron respectively for $I_{app} = 0$, and g_m is related to the resting membrane conductance. $I_{ionic}(V)$ in the QIF model can be thought of as a combination of currents that capture the effects of the leakage current and some of the threshold features of the fast sodium current.

In non-dimensional form (see Appendix 1), the QIF model is

$$\frac{dv_j}{dt} = v_j^2 + I,$$

with a threshold potential v_{th} and a reset potential v_{reset} . For $I > 0$, the T -periodic solution of the QIF model is

$$v_{LC}(t) = \sqrt{I} \tan\left(\sqrt{I}(t + \gamma(v_{reset}))\right) + \beta \delta(t - T), \quad t \in [0, T)$$

where

$$\gamma(v) = \frac{1}{\sqrt{I}} \arctan\left(\frac{v}{\sqrt{I}}\right),$$

with a period of

$$T = \gamma(v_{th}) - \gamma(v_{reset}).$$

The infinitesimal phase-response curve $Z(t)$ for the QIF model is

⁷ Note that the “resting threshold” potential V_T is different than the spike-reset threshold v_{th} .

$$Z(t) = \begin{cases} \frac{1}{I} \cos^2(\sqrt{I}(t + \gamma(v_{reset}))), & 0 < t < T \\ 0, & t = 0, T \end{cases}.$$

GIF dynamics: The periodic solution for general integrate-and-fire (GIF) dynamics cannot be obtained explicitly, but it can be shown that iPRC $Z(t)$ for any single-variable integrate-and-fire model is equal to the reciprocal of the derivative of the membrane potential during the oscillations

$$Z(t) = \begin{cases} (v'_{LC}(t))^{-1}, & 0 < t < T \\ 0, & t = 0, T \end{cases}.$$

During the spike-and-reset phase at $t = 0, T$, we set $Z(t)$ to 0 in all cases. This assumes that during the spike, the cell is not affected by external perturbations (e.g. due to coupling). This is a reasonable assumption because the input conductance is extremely high during spikes, and this renders the cell insensitive to external perturbations.

Note that, outside of the spike, the iPRC $Z(t)$ for any single-variable integrate-and-fire model is strictly positive, and therefore positive currents will always phase advance the cell. This is a characteristic of many neuronal oscillators, especially at low firing rates, and is referred to as type I phase resetting (Ermentrout, 1996; Hansel et al., 1995).

2.2 Phase models for Integrate-and-Fire cells

Plugging the expressions for $Z(t)$ and $v_{LC}(t)$ into the equations for the phase model (equations (eq: H) and (eq: G)) yields the G -function $G(\varphi)$ for the IF models. Note that because of the threshold discontinuity in the “periodic” solution, the integral must be defined in a piecewise manner

$$G(\varphi) = H(-\varphi) - H(-(T - \varphi)) \quad \dots \quad (\text{eq: } G_{IF}).$$

where

$$H(-\varphi) = \frac{1}{T} \int_0^{\varphi^-} Z(t)(v_{LC}(t + T - \varphi) - v_{LC}(t))dt + \frac{1}{T} \int_{\varphi^+}^T Z(t)(v_{LC}(t - \varphi) - v_{LC}(t))dt + \frac{1}{T} \beta Z(\varphi),$$

... (eq: H_{IF}).

Note that $H(-\varphi)$, and therefore $G(\varphi)$, is a linear combination of terms describing the subthreshold effects and the suprathreshold spike effects: (1) The terms with the integrals accounts for all subthreshold activity including the reset, and (2) the term that is scaled by β accounts for the effect of the suprathreshold portion of the spike, i.e.,

$$H_{spike}(-\varphi) = \frac{1}{T} \int_{\varphi^-}^{\varphi^+} Z(t)(\beta\delta(t - \varphi))dt = \frac{1}{T}\beta Z(\varphi)$$

As stated in section 1.2, the stability of the phase-locked states φ^* is given by the sign of $G'(\varphi^*)$. However, for $\beta \neq 0$, $G(\varphi)$ is discontinuous at $\varphi = 0, T$. In this case, $G(0) < 0$ (and $G(T) > 0$) implies stability of the synchronous state.

2.3 Phase-locking in a pair of electrically coupled LIF cells

For the LIF model, the G -function is

$$G(\varphi) = \begin{cases} \frac{2}{T}(\varphi \sinh(T - \varphi) - (T - \varphi) \sinh(\varphi)) + \frac{\beta}{TI}(e^\varphi - e^{T-\varphi}), & 0 < \varphi < T \\ 0, & \varphi = 0, T \end{cases} \quad \dots \text{ (eq: } G_{LIF}\text{)}$$

Figure 2 plots voltage profiles (v_{LC}), iPRCs (Z), and the corresponding G -functions for $I = 1.15$ and $I = 1.5$ with $\beta = 0.1$. The G -function reveals that that both the synchronous state $\varphi = 0, T$ and the anti-phase state $\varphi = T/2$ are stable at $I = 1.15$, whereas only the synchronous state $\varphi = 0, T$ is stable at $I = 1.5$. These results can be understood by considering equation (eq: G_{LIF}).

The phase-locked states and their stability are determined by a competition between the subthreshold portion and suprathreshold portion of the G -function (the solid and dashed grey curves in Figure 2, respectively). The subthreshold portion of the G -function (obtained by setting $\beta = 0$ in equation (eq: G_{LIF})) is always positive in $0 < \varphi < T/2$ and negative in $T/2 < \varphi < T$. This implies that the subthreshold dynamics always have a desynchronizing effect, forcing the coupled LIF cells towards the anti-phase state. Conversely, the suprathreshold (spike) portion of the G -function is always negative in $0 < \varphi < T/2$ and positive in $T/2 < \varphi < T$, and therefore the spike always acts to stabilize the synchronous state $\varphi = 0, T$ and destabilize the anti-phase state $\varphi = T/2$. The delta-function spike causes

the synchronous state to be always stable. However, at low frequencies (I just above 1), the subthreshold term, and therefore the anti-phase state, dominates, i.e., almost all initial conditions evolve to the anti-phase state. As the frequency increases (with increased I), the relative magnitude of the spike effect increases and eventually destabilizes the anti-phase state.

The phase-locked states φ^* over an interval of I for $\beta = 0.1$ are plotted in Figure 3. As pointed out in Figure 2, both the synchronous and the anti-phase states are stable in the case of $I=1.15$, but if I is increased to $I=1.5$ only the synchronous state is stable. In general, at high values of I , the only stable state is the synchronous state, and at sufficiently low I , stable synchronous and anti-phase states coexist. The anti-phase state loses its stability via a subcritical pitchfork bifurcation at the critical value I^* , which depends upon the value of β .

By considering $G'(T/2)$, one can obtain the relationship between the critical value I^* and β analytically

$$\beta = \left(I^* - \frac{1}{2}\right) \ln\left(\frac{I^*}{I^* - 1}\right) - 1 = \frac{T/2}{\tanh(T/2)} - 1 \quad \dots \quad (eq: bI)$$

I^* increases as β decreases, as is seen in Figure 4. This implies that, when the electrotonic effect of the delta-function spikes is weak, anti-phase persists for a larger range of intrinsic frequencies. As the spike effect vanishes ($\beta \rightarrow 0$), the critical current at which the anti-phase state loses stability I^* goes to infinity and the unstable steady states approach the synchronous state. This effectively leaves the anti-phase state as the only stable solution for all I (as mentioned above for $\beta = 0$).

The asynchrony at low frequencies can be understood in terms of the effect of the fast repolarization (reset) of the LIF cells and the shape of their iPRC $Z(t)$. Consider two coupled cells with a small phase difference. During the slow depolarization towards threshold, the membrane potential in the lagging cell is slightly less than that in the leading cell. Consequently, there is a small positive (depolarizing) current in the lagging cell that flows from the leading cell due to the electrical coupling. This current speeds up the lagging cell and slows down the leading cell, which acts to synchronize the cells. However, because the voltage differences are small, the electrotonic current is small and the synchronizing effect of this portion of the subthreshold activity is small. Once the leading cell reaches threshold, it fires and is immediately reset. If the spike does not instantaneously synchronize the cells, the voltage of the leading cell is now below that of the lagging cell, and the electrical coupling current switches direction. Now, coupling acts to impede the increase to threshold of the lagging cell and to speed up the leading cell.

Because the potential difference between the cells is large and the sensitivity of the cells is highest around threshold, the lagging cell is substantially delayed before it fires. This desynchronizing effect is so strong at low firing rates (for which the cells are very sensitive at threshold) that it overcomes the previous synchronizing effect and therefore causes the net effect of coupling over an entire period to be desynchronizing.

2.4 Phase-locking of a pair of electrically coupled GIF/QIF cells

The LIF model highlights how the iPRC and membrane potential (spike, reset and subthreshold portions) combine to generate the phase-locking characteristics of electrically coupled cells. However, LIF dynamics are somewhat limited. In particular, the iPRCs of LIF cells are always increasing and concave up with a maximum at $\varphi \rightarrow T$, i.e., as the membrane potential increases towards threshold, the cell is increasingly sensitive to perturbations and the rate of this increasing sensitivity is itself increasing. Therefore, it is not possible to look for general rules for how the shapes of the iPRC and the membrane potential affect synchronization patterns. We will now consider the GIF models, which allow for a richer set of iPRC shapes. In particular, we will examine how the ‘skewness’ of the PRC (as measured by the location of peak) affects phase-locking. The QIF model will be used to provide specific examples.

Figure 5 plots the voltage profiles (v_{LC}), the iPRCs (Z) and the corresponding G -functions for the QIF model with three different parameter sets. In all cases, $I = 0.1$, $\beta = 0.13$, and $v_{th} - v_{reset} = 3.0$, but v_{reset} is -2.85 , -1.50 , and -0.15 in a, b, and c respectively. Note that the iPRC changes from having a rightward skew of the peak in (a) to being symmetric in (b) to having a leftward skewed peak in (c). Associated with these changes in the iPRCs are changes in the stability of the phase-locked states. The G -function associated with the rightward skewed iPRC shows that both the synchronous state $\varphi = 0, T$ and the anti-phase state $\varphi = T/2$ are stable, although the anti-phase state is dominant. The G -function associated with the symmetric iPRC shows that only the synchronous state $\varphi = 0, T$ is stable. The G -function associated with the leftward skewed iPRC shows that only the anti-phase state $\varphi = T/2$ is stable.

Pfeuty et al. (2003) noted that the skewness of the iPRC has a substantial influence on the stability of the phase-locked states, and they extensively examined how the skewness affected the stability of the anti-phase state of the QIF model. Recall that the stability of the anti-phase state is given by the sign of $G'(T/2) = -2 H'(T/2)$. Therefore, to see how the above changes in the stability of the anti-phase state arise, we can examine how the shape of the iPRC affects $G'(T/2)$. By differentiating equation (eq: G_{if}) with respect to φ and evaluating at $\varphi = T/2$, we see that

$$G' \left(\frac{T}{2} \right) = G'_{sub} \left(\frac{T}{2} \right) + G'_{reset} \left(\frac{T}{2} \right) + G'_{spike} \left(\frac{T}{2} \right) \quad \dots \quad (eq: G')$$

where

$$G'_{sub} \left(\frac{T}{2} \right) = 2 \left(-\frac{1}{T} \int_0^{T/2} Z(t) v'_{LC} \left(t + \frac{T}{2} \right) dt - \frac{1}{T} \int_{T/2}^T Z(t) v'_{LC} \left(t - \frac{T}{2} \right) dt \right),$$

$$G'_{reset} \left(\frac{T}{2} \right) = 2 \left(\frac{1}{T} Z \left(\frac{T}{2} \right) (v_{th} - v_{reset}) \right),$$

$$G'_{spike} \left(\frac{T}{2} \right) = 2 \left(\frac{1}{T} \beta Z' \left(\frac{T}{2} \right) \right).$$

G'_{sub} contains the influence of the intervals of subthreshold depolarization, G'_{reset} contains the influence of the reset from v_{th} to v_{reset} , and G'_{spike} contains the influence of the delta-function spike of strength β . Because $Z \geq 0$ and $v'_{LC} \geq 0$ for all IF models, G'_{sub} is always negative, indicating that the subthreshold depolarization phase in the oscillations always acts to stabilize anti-phase activity. On the other hand, the reset term G'_{reset} is always positive, and therefore the instantaneous reset always acts to destabilize anti-phase activity. Note that this was the case with the LIF model. The spike term G'_{spike} shows that the delta-function spikes act to stabilize anti-phase activity if and only if the iPRC (Z) has a negative slope at $\varphi^* = T/2$. For LIF, $Z'(T/2) > 0$ and spikes always act to synchronize activity. For the QIF, $Z'(T/2) > 0$ whenever the iPRC has a rightward skew (i.e., when $|v_{reset}| > |v_{th}|$), and $Z'(T/2) < 0$ whenever the iPRC has a leftward skew (i.e., when $|v_{reset}| < |v_{th}|$). Thus, spikes act to destabilize anti-phase activity whenever the iPRC has a rightward skew and stabilize anti-phase whenever the iPRC has a leftward skew.

Figure 6 depicts the stability of anti-phase activity for an electrically coupled QIF cell pair in v_{reset} vs frequency (f) parameter space with $v_{th} - v_{reset} = 3.0$. Figure 6a shows the case for $\beta = 0$, which is $G'_{sub} + G'_{reset}$. It shows that the net subthreshold activity acts to destabilize the anti-phase state at all frequencies when the iPRC is symmetric $v_{reset} = -v_{th}$. However, as the magnitude of $v_{th} - v_{reset}$ increases, or equivalently the skewness of the iPRC increases in either direction, the influence of the net subthreshold activity on the anti-phase state becomes stabilizing. Figure 6b shows the results of adding the spike term G'_{spike} to the subthreshold terms. Recall that spikes act to stabilize the anti-phase state when iPRCs skewed to the left ($v_{reset} > -1.5$, i.e., to the right of the dotted line) and destabilize the anti-phase state when iPRCs skewed to the right ($v_{reset} < -1.5$, i.e., to the left of the dotted line).

Furthermore, the spike has a greater effect at higher frequencies. Thus, for iPRCs skewed to the left, anti-phase is unstable at low frequencies, but it becomes stable as the frequency increases, or for iPRCs skewed highly to the left, anti-phase is stable for all frequencies. For iPRCs skewed to the right, anti-phase is stable at low frequencies, but it becomes unstable as the frequency increases. Note that the LIF model has iPRCs similar to those in this latter parameter regime and exhibits equivalent behavior.

A similar analysis can be implemented to determine stability of the synchronous state (Lewis, unpublished results). When the spike effect is included ($\beta > 0$), the synchronous state is stable if $G(\varphi) < 0$, which is the case whenever $Z(0) < Z(T)$. This always holds for the LIF model. It also holds for the QIF model when the iPRC is skewed to the right, but the spike effect acts to destabilize the synchronous state when the iPRC is skewed to the left.

Summary:

Analytical tractability of the IF models has allowed us to establish a clear link between the phase-locking of coupled cells and the shape of the iPRC and to identify the relative contributions of the various different phases in the oscillations. The LIF model showed that only synchrony was stable at higher frequencies, but at low frequencies, the sharp reset (repolarization) and the high sensitivity to input in the late phases had strong desynchronizing effects that led to a stable anti-phase state. The QIF model generalized this result. When the iPRC is skewed to the right (with a peak late in the oscillation cycle), anti-phase was typically stable at low frequencies but destabilized at higher frequencies. Furthermore, increased magnitude of the spike hindered anti-phase activity in this case. On the other hand, the QIF model showed that when the iPRC is skewed to the left (with a peak early in the oscillation cycle), anti-phase was stable at higher frequencies but destabilized at low frequencies. In this case, increased magnitude of the spike promoted anti-phase activity. In terms of the effects of the spike, the sign of $Z'(T/2)$ was the key quantity.

IF models are highly idealized and allow fairly extensive mathematical analyses. However, they also have considerable limitations in terms of linking phase-locking back to biophysical mechanisms. For example, unlike real cells or conductance-based models, the phase response curve and the membrane potential always have the relationship $Z(t) = 1/v'_{LC}(t)$, and the iPRCs of IF models are strictly positive (i.e., they are always type I and never type II). Thus, it is necessary to consider conductance-based models to acquire insight into the biophysical mechanisms of synchronization.

3. Single-Compartment Conductance-based Models for Electrically Coupled Cell-Pairs

A major goal is to determine the role that specific intrinsic membrane conductances play in shaping the synchronization patterns of electrically coupled cells. To do this, we must consider phase-locking in conductance-based models of neurons. However, key insights provided by IF models can be used to guide the examination of these more complex, biophysically-based models.

The conductance-based models that we will consider in this section are single-compartment models given by the Hodgkin-Huxley formalism

$$\begin{aligned} C \frac{dV_j}{d\tilde{t}} &= -I_{ionic,j}(V_j, m_j, h_j, n_j, \dots) + I_{app,j} + g_{gap}(V_k - V_j), \\ \frac{dy_j}{d\tilde{t}} &= \frac{1}{\tau(V_j)}(y_\infty(V_j) - y_j), \quad y_j = m_j, h_j, n_j, \dots \quad \dots \text{ (eq: HH)}, \end{aligned}$$

where $I_{ionic,j}$ is the sum of the various different ionic conductances in the model neuron and $y_j = m_j, h_j, n_j, \dots$ are the gating variables for the conductances.

Pfeuty et al. (2003) is perhaps the most extensive modeling study on how intrinsic conductances affect phase-locking of electrically coupled cells. In a set of numerical simulations of a conductance-based model of a spiking neuron, Pfeuty et al. found that the persistent sodium conductance promoted anti-phase activity (or more generally asynchronous activity), whereas a fast potassium conductance and a slow potassium conductance both promoted synchrony. Using the insight gained from the QIF modeling results, Pfeuty et al. noted that these trends could be understood in terms of their effects on the skew of the iPRC. They showed that increasing the potassium conductances led to a rightward shift in the peak of the iPRC (see also Crook et al., 1998b; Ermentrout et al., 2001), whereas the persistent sodium conductance shifted the peak to the left. Pfeuty et al. pointed out that these effects on the iPRCs can be understood in the following way: The potassium conductances increase refractoriness of a neuron after the spike, and therefore they reduce the responsiveness of the neuron to external perturbations during the first portion of the period, shifting the maximum of the iPRC toward latter phases. On the other hand, the persistent sodium conductance is activated near rest and depolarizing perturbations boost its activation, and thus it increases the responsiveness of the neuron after a spike and shifts the maximum of the iPRC toward first half of the period. The upshot of Pfeuty et al. (2003) was that the refractory effects of the potassium conductances and the boosting effects of the persistent sodium conductance are responsible for how these conductances alter the phase-locking dynamics of electrically coupled neurons.

Curiously, Mancilla et al. (2007) found that both potassium conductances in the Erisir et al. (1999) model for neocortical FS cells (i.e., a Kv1.3-conductance and a Kv3.2/3-conductance) actually promoted anti-phase behavior. This apparent disagreement between the Mancilla et al. (2007) and Pfeuty et al. (2003) can be resolved by reconsidering the results from the QIF model. Figure 6b indicates that a decrease in v_{reset} (a rightward skew of the iPRC) will destabilize anti-phase at higher frequencies, but it will stabilize anti-phase at lower frequencies. Thus, assuming that it will cause a rightward skew of the iPRC, an increase in the potassium conductances should have different effects on anti-phase in different frequency regimes. Indeed, the anti-phase that Pfeuty et al. considered was at higher firing rates, whereas the anti-phase that Mancilla et al. considered was at lower frequencies. This implies a modified rule of thumb for the effects of potassium conductances: potassium conductances promote synchrony at higher frequencies, but they can promote anti-phase at lower frequencies.

The above explanation, which was motivated by the IF modeling, provides some understanding of how certain conductances affect phase-locking, however it appears not to be the entire story. The actions of these and other conductances can sometimes be more subtle. For example, potassium conductances can have various influences on phase-locking of electrically coupled neurons. Nomura et al. (2003) studied a model of fast-spiking (FS) interneurons with a strong Kv3.1 conductance and found that it exhibited only stable synchrony over the entire frequency range studied (~5 Hz to 250Hz). They also examined the Hodgkin-Huxley model, which has a large Kv1.1 delayed-rectifier conductance, and found that stable anti-phase and synchronous states co-existed for frequencies up to ~100Hz. On the other hand, DiGarbo et al. (2005) studied another FS interneuron model (modified from Durstewitz et al. 2000) that also had a fast and strong Kv3-like conductance, but they found bistability of the anti-phase state and the synchronous state up to 80 Hz. Ermentrout and Wechselberger (2009) found that the iPRC of the Erisir et al. model for cortical FS interneurons was highly oscillatory at very low frequencies, which gave rise to multistability in cell-pairs and clustering in larger networks of cells. They showed that the slow potassium current (Kv1.3) was at the root of this behavior. Finally, in Mancilla et al. (2007), while both potassium conductances in the FS cell model promoted anti-phase behavior at low frequencies, these potassium conductances had different effects on the iPRC. At 25 Hz, the Kv1 conductance shifted the iPRC peak to the right (and had a visually unperceivable change on the membrane potential), whereas Kv3 conductance shifted the peak in the iPRC to the left (and substantially decreased the spike width and increased the AHP).

In essence, while much insight can be obtained from the explanation based on the skewness of the iPRC, predicting electrically coupled network dynamics from iPRCs alone can be tricky, especially because predictions from the weakly coupled oscillator theory involve both iPRCs and the voltage trajectories via the coupling function. Mancilla et al. (2007) showed that the voltage trajectory can sometimes have a predominant effect over the iPRC in predicting the stability of the anti-phase state in electrically coupled networks of conductance-based models. In particular, by explicitly manipulating the voltage trajectory, they found that an increased spike width and a decreased AHP destabilized the anti-phase state. Thus, spike details as described by conductance-based models also need to be taken into consideration in predicting the output from electrically coupled networks.

One way to start addressing the role of the membrane potential is to exploit the linearity of the integral in the G -function by decomposing v_{LC} into two or more components. We can then consider the corresponding components of $G'(T/2)$ separately. For example, we can consider the influence of the after-hyperpolarization (AHP) by adding an AHP component to the baseline membrane potential, $v_{LC}(t) + v_{AHP}(t)$. The integral for $G'(T/2)$ will separate into two components, and by integrating by parts, we see that

$$\begin{aligned} G'\left(\frac{T}{2}\right) &= -\frac{2}{T} \int_0^T Z(t) \left(v'_{LC}\left(t + \frac{T}{2}\right) + v'_{AHP}\left(t + \frac{T}{2}\right) \right) dt \\ &= -\frac{2}{T} \int_0^T Z(t) v'_{baseline}\left(t + \frac{T}{2}\right) dt + \frac{2}{T} \int_0^T Z'(t) v_{AHP}\left(t + \frac{T}{2}\right) dt . \end{aligned}$$

The second integral term contains the influence of the added AHP on the stability of anti-phase state. It reveals that the AHP will have a stabilizing effect if $Z'(t) > 0$ during the bulk of the AHP (note $v_{AHP}(t) < 0$).

The above discussion clearly demonstrates that, in order to identify the conductances responsible for promoting synchronization, we need to understand how intrinsic membrane conductances shape both the PRCs and membrane potential trajectory of individual cells (Acker et al., 2003; Crook et al., 1998b; Ermentrout et al., 2001; Mancilla et al., 2007; Pfeuty et al., 2003; Stiefel et al., 2009). More work needs to be done to sort this out. Specific questions that need to be addressed are: What do negative lobes do? How do details of activation curves and time constants determine a conductance's effect on phase-locking behavior? How important are the interactions with other conductances?

Another issue to consider is that neurons are not “single somatic compartments”, and some gap junctions are known to be located on dendrites, often quite far from the cell body (Fukuda, 2007). In the next section, we describe work with multi-compartment models that takes into consideration the effect on network dynamics of different gap junction coupling locations.

4. Multi-compartment Models: Effects of Coupling Location and Dendritic Conductances

In this section, we first summarize what has been done and predicted with multi-compartment models in which the dendrites are either passive or active. We then describe the equations and analyses using a three-compartment model for illustrative purposes.

Crook et al. (1998a) were the first to use iPRCs and weakly coupled oscillator theory to understand how the presence of dendrites on individual neurons could affect the activity of neuronal networks. The low-pass filtering effects of dendrites on both membrane potential and iPRCs were described in Lewis & Rinzel (2004), and Goldberg et al. (2007) derived a closed form expression for iPRCs generated by dendritic perturbation (dPRC). Specifically, the passive properties of the dendrites cause a leftward shift and attenuation of the somatic iPRC. What this means is that a negative lobe present in a somatic iPRC (due to a type II model) will no longer exist in the dPRC at a far enough dendritic location, so that one gets a type I response in the dendrite. The leftward shift and attenuation of PRCs can be seen in Pfeuty et al. (2005) for their two-compartment conductance-based model, as well as in Lewis & Rinzel (2004) where a type II response in the soma and a type I response in the dendrite is also apparent in the two-compartment model that they used.

Passive dendrites:

Using a ball-and-stick neuron model, Crook et al. (1998a) extended a somatic neuronal oscillator model to include a thin dendrite. Using the weakly coupled oscillator theory with *chemical* coupling, they showed that stable, phase-locked, synchronous solutions depend on the length of the dendrite and its passive biophysical properties (membrane time constant and length constant). They also used an 11-compartment model of a pyramidal cell (somatic compartment, basal dendrite compartment and nine apical dendrite compartments) and applied the theory to predict phase-locked states. With dendritic coupling, asynchronous, but non-antiphase, stable phase-locking is predicted and shown in their network simulations.

For electrical coupling, Lewis & Rinzel (2004) used a two-compartment model of a fast-spiking cortical neuron (active soma, passive dendrite) to demonstrate how dendritic filtering and the location of gap junctions could alter phase-locking. They showed that stable antiphase patterns can occur at higher frequencies when coupling is in dendritic regions, but when the electrical coupling is somatic, antiphase patterns do not occur at the higher frequencies. As in the chemical coupling case, asynchronous, but non-antiphase, phase-locking is predicted to occur with dendritic coupling. In a series of simulations involving more realistic neuronal morphologies, Saraga & Skinner (2004) built a 372-compartment model of a hippocampal basket cell and examined two-cell networks that were electrically coupled at proximal, middle or distal dendritic locations, in which the dendrites were passive. Asynchronous phase-locked states occurred when the cells were coupled at middle or distal locations, but not when coupled at proximal locations. Moreover, synchrony never occurred in these model neurons at any frequency when the weak electrical coupling occurred at distal locations (Saraga & Skinner, 2004; Saraga et al., 2006).

Active dendrites

It is clear that with the addition of passive dendrites, electrically coupled network output changes. However, the dendrites of neurons contain active voltage-gated channels (Johnson & Narayanan, 2008) and this would also be expected to affect the network output. Goldberg et al. (2007) showed in their analysis that dendritic conductances could be classified as either regenerative (boosting dPRCs and giving more of a leftward shift) or restorative (high pass filtering dPRCs possibly creating a negative portion in the dPRC so that a type II response can occur). Regenerative conductances would include the persistent sodium currents, and restorative conductances would include delayed rectifier potassium currents. Note that these classifications correspond to the results of Pfeuty et al. (2003) that were discussed in the previous section. In two-cell network simulations performed with 372-compartment models in which the dendrites included voltage-gated sodium and delayed rectifier potassium currents, the dPRCs exhibited negative lobes – type II PRCs (Saraga et al., 2006). However, as pointed out by Goldberg et al. (2007), care needs to be taken in making such statements because adding active conductances in the dendrite can affect whether the somatic response is type I or II, and the density of the active conductances would also have an effect. In other words, it becomes more difficult to predict the changes in PRCs as more realistic neurons with active dendrites are considered. Indeed, in examining the effects of cholinergic neuromodulation on PRCs (type II to type I) of modeled cortical neurons, which included a 257-compartment model of a layer II pyramidal neuron, Stiefel et al. (2009) found that the modulation was independent of the perturbation location. That is, the location was not a determining factor in changing the PRC characteristics.

If one takes the next step of applying weakly coupled oscillator theory using the dPRCs, then predictions can be made. This was done by Crook et al. (1998a) in showing that inward and outward currents affected the size of stable phase lags in two-cell networks coupled with excitatory synapses. Saraga et al. (2006) examined how including different densities of voltage-gated sodium and potassium channels in the dendrites affected phase-locked states in electrically coupled networks. They applied weak coupling theory using a three-compartment model, which was a reduced version of their 372-compartment model of a hippocampal basket cell. The density of voltage-gated channels in the dendrites was shown to have a dramatic effect on the phase-locked state, and this could be somewhat correlated with a negative lobe in the dPRC. Specifically, negativity in the dPRC was predicted to give phase-locked states that were asynchronous when electrically coupled at these distal sites.

In moving toward multi-compartment models of neurons that represent both the appropriate morphology as well as biophysical characteristics of the particular cell, Zahid & Skinner (2009) built multi-compartment models of hippocampal interneurons that matched the spike attenuation characteristics measured in these cells, by adjusting the dendritic conductances. These neurons are of particular interest because it is known that gap junctions are present at dendritic locations (Fukuda & Kosaka, 2000). They generated dPRCs and used the theory to predict phase-locked states. By directly comparing theoretical predictions and simulations, they suggested that quantifying the amount of skewness in measured PRCs was a good indicator of whether electrically coupled networks would produce synchronous or asynchronous output. However, as noted earlier (see previous section), one needs to be careful in predicting network dynamics from PRCs alone as details of the voltage trajectory also play a role. Nevertheless, it is helpful to try to make predictions based on PRCs alone.

We now describe the procedure that one can follow in using weakly coupled oscillator theory with multi-compartment models to predict the output from two-cell networks. We first note that with a larger number of compartments in multi-compartment models, PRCs can be obtained by directly perturbing the model. If there are only a few compartments then the iPRC, $Z(t)$, can be obtained by computing the solution to the linearized model system's adjoint equations (see Chapter X), e.g. using XPPAUT (Ermentrout, 2002). However, in working with a reduced model with a minimal number of compartments, it is important to note that the full model's electrotonic characteristics cannot be completely captured (Saraga et al., 2006; Crook et al. 1998a), and this could be critically important in determining the network output.

To illustrate the application of the weak coupling oscillator theory process for a multi-compartment model, let us assume that we have a three-compartment model consisting of a soma (s), a proximal dendrite (pd) and a distal dendrite (dd). The voltage components of the three-compartment model system are given by the following equations for cell 1 (subscript for cell number and superscript for the compartment).

$$\begin{aligned} C \frac{dV_1^s}{dt} &= \gamma(V_1^{pd} - V_1^s) - I_{ionic,1}^s \\ C \frac{dV_1^{pd}}{dt} &= \gamma(V_1^s - V_1^{pd}) + \gamma(V_1^{dd} - V_1^{pd}) - I_{ionic,1}^{pd} \\ C \frac{dV_1^{dd}}{dt} &= \gamma(V_1^{pd} - V_1^{dd}) - I_{ionic,1}^{dd} \end{aligned}$$

where γ is the coupling conductance between connected compartments (assumed to be uniform) in the multi-compartment model cell. Other parameters are defined as in the basic equation (*eq:current*) given in the Introduction. Cell 2 equations would be the same with adjusted cell number subscript. An electrically coupled two-cell network is formed when gap junctions are present between compartments of two different cells (cell 1 and cell 2). In that case, an additional current would be added to the right-hand side of the equation for the appropriate compartment of each cell. If gap junctions are present between the k th compartments of cell 1 and cell 2, then

$$\begin{aligned} I_{gap,1:2}^k &= g_{gap}(V_1^k - V_2^k) \\ I_{gap,2:1}^k &= g_{gap}(V_2^k - V_1^k) \end{aligned}$$

would be added to the cell 1 and cell 2 model equations for the k th compartment respectively.

To apply the weakly coupled oscillator theory to predict what phase-locked states would be present in an electrically coupled two-cell network of multi-compartment model cells, the process has been described for a single compartment model in the introductory Chapter X, but one needs to use the PRC and voltage for the compartment where the coupling occurs.

For example, consider the situation where the gap junction coupling is between the distal dendrites (dd) of cell 1 and cell 2. Let $Z^{dd}(t)$ be the iPRC at that location. Then the dynamics of a pair of electrically coupled cells is given by:

$$\frac{d\psi_q}{dt} = \frac{1}{T} \int_0^T Z^{dd}(\bar{t} + \psi_q) (g_{gap} [V^{dd}(\bar{t} + \psi_p) - V^{dd}(\bar{t} + \psi_q)]) d\bar{t} = g_{gap} H(-(\psi_q - \psi_p))$$

... (eq:C),

where ψ_q is the phase of the q^{th} cell and

$$H(-(\psi_q - \psi_p)) = \frac{1}{T} \int_0^T Z^{dd}(s) [V^{dd}(s - (\psi_q - \psi_p)) - V^{dd}(s)] ds.$$

Thus, the G -function $G(\phi) = g_{gap} [H(-\phi) - H(\phi)]$, which describes the evolution of the phase difference between the two cells ($\phi = \psi_q - \psi_p$), includes properties of the uncoupled cells, the voltage at the dd location, the PRC at the dd location, and the expression of the gap junction coupling. If coupling is at the soma (s) or proximal dendrite (pd) location instead, then Z^s and V^s or Z^{pd} and V^{pd} respectively would be used instead in the above equations.

In Figure 7, we plot the voltage at all three locations and show the resulting Z function (iPRCs) at each of these locations. The iPRC at time zero corresponds to the spike peak in the soma, which does not correspond to peaks in the dendritic locations. This is made clear by the plot in the far right panel of the first row in which voltages at all three locations are plotted. Comparison of the iPRCs at the three locations is shown in the far right panel of the second row. The predicted leftward shift and attenuation can be seen. Also apparent is the development of a negative portion in the PRC with non-somatic perturbations. The dramatic effect on the resulting G -function as the coupling location changes can be seen in the third row of the figure. Parameter values and additional equations are given in Appendix 2.

Example voltage output from a two-cell network in which weak electrical coupling is between distal dendrites of three-compartment neurons is given in the bottom row of Figure 7. Voltage output from each of the three compartments (soma, pd , dd) is shown. For the parameters used in this example in which voltage-gated channels are present in the dendrites, asynchronous output occurs with about a 20% phase lag between the two cells (i.e., about a 10 ms lag for a 47 ms period). This phase lag is predicted by the zero crossing of the G -function which has a negative slope, as given in the third row, third panel of Figure 7. If coupling occurred at a pd or soma location instead, then the G -function would give a prediction of either about 5 ms lag or synchrony respectively – note the zero crossings with negative slope of the G -

function in the first and second panels of the third row of Figure 7. Thus, the location of gap junctions can have a dramatic effect on phase-locked states, and this effect can be predicted using weakly coupled oscillator theory.

5. Summary and Discussion

In this chapter, we have shown how the theory of weakly coupled oscillators can provide insight into the phase-locking behavior of electrically coupled spiking neurons, and we described how synchronization patterns depend on details of both the PRC and voltage trajectory, both being part of the G -function derived in the weak coupling theory. For some idealized models (e.g. integrate-and-fire), detailed analyses can be done to make precise statements about phase-locking behaviors. However, even when the models become more complex with biophysical conductances, multi-compartment structures and active dendrites, phase-locking behaviors can still be predicted from the G -functions. We note that the STRC method, which is another method that uses PRCs to network behavior (as described in Chapter(s) XX), cannot be applied to networks with electrical coupling. This is because the coupling current that flows between the cells is not pulsatile and does not have a characteristic shape. Instead, the current flowing between the cells is present throughout the oscillation cycle and is different for any given phase-difference between the cells.

In this chapter, we have focused on networks of two identical noiseless cells. However, as discussed in introductory Chapter X, the theory of weak coupling can be extended to include heterogeneity, noise and large numbers of cells. The maxima of G -functions determine the robustness of the phase-locked states to heterogeneity (e.g. Mancilla et al., 2007), and the effects of additive white noise on the distribution of phase-differences is given by a formula that involves integrals of the G -functions (Pfeuty et al 2005; see equation (*equ:distn*) in Chapter X). Therefore, by examining how the shapes of Z and V_{LC} affect these quantities, one can explore the effects of noise and heterogeneity in electrically coupled networks.. Perhaps not so surprisingly, the basic conclusions from the identical noiseless cell-pairs largely carry over to these more complicated situations. For example, Pfeuty et al. (2003) observed that large heterogeneous networks of QIF neurons displayed the same phase-locking regimes that they found for QIF cell-pairs, except for regimes that occurred for particularly small regions of parameter space. We should note however that fundamentally new behavior can be observed in large networks with spatially localized connectivity. For instance, Kazanci & Ermentrout (2007) showed transitions from global synchrony to travelling wave activity in a network with localized weak electrical coupling.

Strictly speaking, weakly coupled oscillator theory only applies when the coupling is sufficiently weak. However, qualitative results and general insights obtained using this theory often hold for moderate coupling strengths. For example, weakly coupled oscillator theory was used to determine three different regions of phase-locking behaviors for varying levels of active dendrites in multi-compartment models. When larger electrical coupling strengths were explored with simulations, these different regions were still apparent (Saraga et al., 2006). Furthermore, we note that techniques to explore strong electrical coupling are being developed using piecewise linear models (Coombes, 2008).

Other Considerations, Biological Details and Future Work

Ultimately, we would like to obtain a functional understanding of the roles played by gap junctional coupling in cortical systems. The goal of this chapter was to characterize synchronization patterns brought about by electrically coupled networks using the theory of weakly coupled oscillators. The use of theory is to expand our understanding and insight over that obtained from direct numerical simulations alone, to help obtain a functional understanding. However, it is sometimes the case that biologically detailed and realistic simulations can provide functional insights that are strengthened by subsequent theoretical work or can be explained by previous theoretical work. For example, work by Traub et al. (1999) using large, detailed network simulations predicted the need for axo-axonic gap junctions for the generation of high frequency population oscillations. Subsequent theoretical work by Lewis & Rinzel (2000) using cellular automata was able to explain how the resulting network frequencies occurred. In a large, detailed network of striatal fast-spiking cells, Hjorth et al. (2009) suggested that gap junctions played more of a shunting rather than a synchronizing role. This shunting aspect of gap junction coupling in large interconnected networks was examined by Amitai et al. (2002) in neocortical interneurons. These detailed electrically coupled network models included other details involving chemical synaptic input characteristics relevant for the particular situation.

The presence of both electrical and chemical synapses has motivated several modeling and theoretical works (e.g., Gao & Holmes, 2007; Kazanci & Ermentrout, 2007; Kopell & Ermentrout, 2004; Lewis & Rinzel, 2003; Pfeuty et al., 2005; Skinner et al., 1999). These works show the increased richness that emerges in these networks. What remains to be explored is how realistic spatial architecture of electrically coupled networks (Amitai et al., 2002) affects resulting synchronization patterns.

APPENDIX 1

Leaky Integrate-and-fire (LIF)

For the standard leaky integrate-and-fire (LIF), the ionic current is described only by the leakage current

$$I_{ionic}(V) = g_m(V - V_r),$$

where V_r is the reversal potential of the leakage current, g_m is the membrane leakage conductance of the cell. For $I_{app} > g_l(V_{th} - V_r)$, the \tilde{T} -periodic solution is

$$\begin{aligned} V_{LC}(\tilde{t}) &= \left(\frac{I_{app}}{g_m} + V_r \right) - \left(\frac{I_{app}}{g_l} + V_r - V_{reset} \right) e^{-\frac{g_m \tilde{t}}{C_m}} \\ &= V_{ss} - (V_{ss} - V_{reset}) e^{-\frac{\tilde{t}}{\tau}}, \end{aligned}$$

where

$$V_{ss} = \left(\frac{I_{app}}{g_m} + V_r \right), \quad \tau = \frac{C_m}{g_m},$$

and the period is

$$\tilde{T} = \tau \ln \left(\frac{V_{ss} - V_{reset}}{V_{ss} - V_{th}} \right).$$

The infinitesimal phase-response curve for the LIF model (Hansel et al., 1995; Neltner et al., 2000) is

$$\tilde{Z}(\tilde{t}) = \begin{cases} \frac{\tau}{V_{ss} - V_{reset}} \exp\left(\frac{\tilde{t}}{\tau}\right), & 0 < \tilde{t} < \tilde{T} \\ 0, & \tilde{t} = 0, \tilde{T} \end{cases}.$$

Non-dimensionalization: By taking

$$v_j = \frac{V_j - V_r}{V_{th} - V_r}, \quad t = \frac{\tilde{t}}{C_m/g_m},$$

and

$$I = \frac{I_{app}}{g_m(V_{th} - V_r)}, \quad \beta = \frac{\tilde{\beta}}{g_m(V_{th} - V_r)}, \quad g_{gap} = \frac{\tilde{g}_{gap}}{g_m}, \quad v_{reset} = \frac{V_{reset} - V_r}{V_{th} - V_r},$$

we obtain the following non-dimensional LIF model for electrically coupled cells

$$\frac{dv_j}{d\tilde{t}} = -v_j + I + g_{gap}(v_k - v_j),$$

When v_j reaches a threshold potential 1, cell j fires a δ -function spike of magnitude β after which v_j is reset to the potential 0.

Quadratic Integrate-and-fire (QIF)

For the quadratic integrate-and-fire (QIF), the ionic current is

$$I_{ionic}(V) = g_m \frac{(V_T - V)(V - V_R)}{(V_T - V_R)} = g_m \frac{(V - \bar{V})^2}{V_-} - I_b,$$

where V_R and V_T are the resting potential and “threshold” potential of the neuron respectively for $I_{app} = 0$, and g_m is related to the resting membrane conductance. $\bar{V} = (V_T + V_R)/2$ and $V_- = V_T - V_R$. $I_b = g_m \bar{V}^2 / V_-$ acts as an intrinsic bias current. $I_{ionic}(V)$ can be thought of as a combination of currents that captures the effects of the leakage current and some of the threshold aspects related to the fast sodium current. For $I_{app} > I_b$, the \tilde{T} -periodic solution is

$$V_{LC}(\tilde{t}) = \bar{V} + V_- \sqrt{I} \tan\left(\sqrt{I} \frac{\tilde{t}}{\tau} + \gamma(V_{reset})\right),$$

where

$$I = \frac{I_{app} - I_b}{g_m V_-}, \quad \tilde{\gamma}(V) = \frac{1}{\sqrt{I}} \arctan\left(\frac{V - \bar{V}}{V_- \sqrt{I}}\right),$$

with a period of

$$\tilde{T} = \tau(\tilde{\gamma}(V_{th}) - \tilde{\gamma}(V_{reset})).$$

The infinitesimal phase-response curve $Z(\tilde{t})$ for the QIF model is

$$\tilde{Z}(\tilde{t}) = \begin{cases} \frac{\tau}{V_-} \frac{1}{\sqrt{I}} \cos^2 \left(\sqrt{I} \frac{\tilde{t}}{\tau} + \tilde{\gamma}(V_{reset}) \right), & 0 < \tilde{t} < \tilde{T} \\ 0, & \tilde{t} = 0, \tilde{T} \end{cases}$$

Non-dimensionalization: By taking

$$v_j = \frac{V_j - \bar{V}}{V_-}, \quad t = \frac{\tilde{t}}{C_m/g_m},$$

and

$$\beta = \frac{\tilde{\beta}}{g_m V_-}, \quad g_{gap} = \frac{\tilde{g}_{gap}}{g_m}, \quad v_{reset} = \frac{V_{reset} - \bar{V}}{V_-}, \quad v_{th} = \frac{V_{th} - \bar{V}}{V_-},$$

we obtain the following non-dimensional QIF model:

$$\frac{dv_j}{dt} = v_j^2 + I + g_{gap}(v_k - v_j),$$

When v_j reaches a threshold potential v_{th} , cell j fires a δ -function spike of magnitude β after which v_j is reset to the potential v_{reset} .

APPENDIX 2

Additional Equations and Parameter Values used for three-compartment model

Parameter	Value	Units
γ	0.5	mS/cm ²
C	0.8	μ F/cm ²
g_{Na}^s	184	mS/cm ²
g_{Na}^{dd}, g_{Na}^{pd}	2.76	mS/cm ²

g_K^s	140	mS/cm ²
g_K^{dd}, g_K^{pd}	2.1	mS/cm ²
g_L	0.0245	mS/cm ²
V_{Na}	55	mV
V_K	-90	mV
V_L	-60	mV
g_{gap}	0.02	mS/cm ²

The following equations are the same for each compartment in each of cell 1 and 2, with parameter values as given in the above table.

$$I_{ionic} = g_{Na} m^3 h (V - V_{Na}) + g_K n^4 (V - V_K) + g_L (V - V_L)$$

$$\frac{dm}{dt} = \alpha_m (1 - m) - \beta_m m$$

$$\frac{dh}{dt} = \alpha_h (1 - h) - \beta_h h$$

$$\frac{dn}{dt} = \alpha_n (1 - n) - \beta_n n$$

where

$$\alpha_m = -0.1(V + 35) / (\exp[-0.1(V + 35)] - 1)$$

$$\beta_m = 4 \exp[-(V + 60)/18]$$

$$\alpha_h = 0.07 \exp[(V + 58)/20]$$

$$\beta_h = 1 / (\exp[-0.1(V + 28)] + 1)$$

$$\alpha_n = -0.01(V + 34) / (\exp[-0.1(V + 34)] - 1)$$

$$\beta_n = 0.125 \exp[-(V + 44)/80]$$

Acknowledgements: TJJ was supported by the National Science Foundation under grants DMS-09211039 and DMS-0518022. FKS thanks the Natural Sciences and Engineering Research Council of Canada for support.

References:

- Acker, C.N., N Kopell, N., & White, J.A. (2003). Synchronization of strongly coupled excitatory neurons: Relating network behavior to biophysics. *Journal of Computational Neuroscience*, 15(1), 71-90.
- Amitai, Y., Gibson, J.R., Beierlein, M., Patrick, S.L., Ho, A.M., Connors, B.W., & Golomb, D. (2002). The spatial dimensions of electrically coupled networks of interneurons in the neocortex. *Journal of Neuroscience*, 22(10), 4142-4152.
- Bem, T., Le Feuvre, Y., Rinzel, J., & Meyrand, P. (2005) Electrical coupling induces bistability of rhythms in networks of inhibitory spiking neurons. *European Journal of Neuroscience*, 22, 2661– 2668.
- Bennett, M.V.L. (1977). Electrical transmission: a functional analysis and comparison to chemical transmission. In: *Handbook of Physiology. The Nervous System. Cellular Biology of Neurons*. (Sect. 1, Vol. I, pt. 1, pp. 357–416). Bethesda, MD: American Physiological Society.
- Bennett, M.V.L. (2000). Seeing is relieving: electrical synapses between visualized neurons. *Nature*, 3(1), 7-9.
- Bennett, M.V.L., & Zukin, R.S. (2004). Electrical coupling and neuronal synchronization in the mammalian brain. *Neuron*, 41, 495-511.
- Chow, C.C., & Kopell, N. (2000). Dynamics of spiking neurons with electrical coupling. *Neural Computation*, 12, 1643-1678.
- Coomes S. (2008). Neuronal networks with gap junctions: A study of piece-wise linear planar neuron models. *SIAM Journal of Applied Dynamical Systems*, 7, 1101-1129.
- Connors, B.W. & Long, M.A. (2004). Electrical synapses in the mammalian brain. *Annual Reviews of Neuroscience*, 27, 393-418.
- Crook, S.M., Ermentrout, G.B., & Bower, J.M. (1998a) Dendritic and synaptic effects in systems of coupled cortical oscillators. *Journal of Computational Neuroscience*, 5(3), 315-329.
- Crook, S.M., Ermentrout, G.B., & Bower, J.M. (1998b) Spike frequency adaptation affects the synchronization properties of networks of cortical oscillators. *Neural Computation*, 10, 837-854.
- Cymbalyuk, G.S., Nikolaev, E.V., & Borisyuk, R.M. (1994). In-phase and antiphase self-oscillations in a model of two electrically coupled pacemakers. *Biological Cybernetics*. 71, 153-160.
- Di Garbo, A., Panarese, A., & Chillemi, S. (2005). Gap junctions promote synchronous activities in a network of inhibitory interneurons. *Biosystems* 79, 91-99.
- Durstewitz, D., Seamans, J.K., & Sejnowski, T.J. (2000). Dopamine-mediated stabilization of delay-period activity in a network model of prefrontal cortex. *Journal of Neurophysiology*, 83, 1733–1750.
- Erisir, A., Lau, D., Rudy, B., & Leonard, S. (1999). Function of specific K⁺ channels in sustained high-frequency firing of fast-spiking neocortical cells. *Journal of Neurophysiology*, 82, 2476–2489.
- Ermentrout, G.B. (1996). Type I membranes, phase resetting curves, and synchrony. *Neural Computation*, 8(5), 979-1001.

- Ermentrout, G.B., Pascal, M., & Gutkin, B. (2001). The effects of spike frequency adaptation and negative feedback on the synchronization of neural oscillators. *Neural Computation*, 8(6), 1285-1310.
- Ermentrout, G.B. (2002). *Simulating, Analyzing, and Animating Dynamical Systems: A Guide to XPPAUT for Researchers and Students*. Philadelphia: SIAM.
- Ermentrout, G.B., & Wechselberger, M. (2009). Canards, clusters, and synchronization in a weakly coupled interneuron model. *SIAM Journal of Applied Dynamical Systems*, 8(1), 253-278.
- Fukuda, T. (2007). Structural organization of the gap junction network in the cerebral cortex. *Neuroscientist*, 13, 199-207.
- Fukuda, T., & Kosaka, T. (2000). Gap junctions linking the dendritic network of GABAergic interneurons in the hippocampus. *Journal of Neuroscience*, 20, 1519-1528.
- Galarreta, M., & Hestrin, S. (2001). Electrical synapses between GABA-releasing interneurons. *Nature Reviews Neuroscience*, 2, 426-433.
- Gao, J., & Holmes, P. (2007). On the dynamics of electrically-coupled neurons with inhibitory synapses. *Journal of Computational Neuroscience*, 22, 39-61.
- Glass, L., & Mackey, M.C. (1998). *From Clocks to Chaos: The Rhythms of Life*. Princeton University Press.
- Goldberg, J.A., Deister, C.A., & Wilson, C.J. (2007). Response properties and synchronization of rhythmically firing dendritic neurons. *Journal of Neurophysiology*, 97, 208-219.
- Gutkin, B.S., Ermentrout, G.B., & Reyes, A.D. (2005). Phase-response curves give the responses of neurons to transient inputs. *Journal of Neurophysiology*, 94, 1623-1635.
- Hansel, D., Mato, G., & Meunier, C. (1995). Synchrony in excitatory neural networks. *Neural Computation*, 7, 307-337.
- Hjorth, J., Backwell, K.T., & Kotaleski, J.H. (2009). Gap junctions between striatal fast-spiking interneurons regulate spiking activity and synchronization as a function of cortical activity. *Journal of Neuroscience*, 29(16), 5276-5286.
- Hormuzdi, S.G., Filippov, M.A., Mitropoulou, G., Monyer, H., & Bruzzone, R. (2004). Electrical synapses: a dynamic signaling system that shapes the activity of neuronal networks. *Biochimica et Biophysica Acta*, 1662, 113-137.
- Johnston, D., & Narayanan, R. (2008). Active dendrites: colorful wings of the mysterious butterflies. *Trends in Neuroscience*, 31(6), 309-16.
- Kazanci, F.G., & Ermentrout, G.B. (2007). Pattern Formation in an Array of Oscillators with Electrical and Chemical Coupling. *SIAM Journal of Applied Mathematics*, 67, 512-529.
- Kopell, N., & Ermentrout, G.B. (2004). Chemical and electrical synapses perform complementary roles in the synchronization of interneuronal networks. *Proceedings of the National Academy of Science USA*, 101(43), 15482-15487.

- Kuramoto, Y. (1984). *Chemical Oscillations, Waves, and Turbulence*. New York: Springer-Verlag.
- Latham, P.E., Richmond, B.J., Nelson, P.G., & Nirenberg, S. (2000). Intrinsic dynamics in neuronal networks. I. Theory. *Journal of Neurophysiology*, 83(2), 808-827.
- Lewis, T.J., & Rinzel, J. (2000). Self-organized synchronous oscillations in a network of excitable cells coupled by gap junctions. *Network: Computation in Neural Systems*, 11(4), 299-320.
- Lewis, T.J., & Rinzel, J. (2003). Dynamics of spiking neurons connected by both inhibitory and electrical coupling. *Journal of Computational Neuroscience*, 14, 283-309.
- Lewis, T.J., & Rinzel, J. (2004). Dendritic effects in networks of electrically coupled fast-spiking interneurons. *Neurocomputing*, 58-60, 145-150.
- Mancilla, J.G., Lewis, T.J., Pinto, D.J., Rinzel, J., & Connors, B.W. (2007). Synchronization of electrically coupled pairs of inhibitory interneurons in neocortex. *Journal of Neuroscience*, 27(8), 2058-2073.
- Meier, C., & Dermietzel, R. (2006). Electrical synapses – gap junctions in the brain. *Results and Problems in Cell Differentiation*, 43, 99-128.
- Neltner, L., Hansel, D., Mato, G., & Meunier, C. (2000). Synchrony in heterogeneous networks of spiking neurons. *Neural Computation*, 12, 1607-1641.
- Nomura, M., Fukai, T., & Aoyagi, T. (2003). Synchrony of fast-spiking interneurons interconnected by GABAergic and electrical synapses. *Neural Computation*, 15, 2179-2198.
- Pfeuty, B., Golomb, D., Mato, G., & Hansel, D. (2003). Electrical synapses and synchrony: The role of intrinsic currents. *Journal of Neuroscience*, 23(15), 6280-6294.
- Pfeuty, B., Golomb, D., Mato, G., & Hansel, D. (2003). The combined effects of inhibitory and electrical synapses in synchrony. *Neural Computation*, 17, 633-670.
- Rinzel, J., & Ermentrout, G.B. (1988). Analysis of neural excitability and oscillations (chp.7, pp251-191). In: *Methods in Neuronal Modeling: From Ions to Networks* (2nd ed., C.Koch, I.Segev eds). Cambridge MA: MIT Press.
- Saraga, F., & Skinner, F.K. (2004). Location, location , location (and density) of gap junctions in multi-compartment models. *Neurocomputing*, 58-60, 713-719.
- Saraga, F., Ng, L., & Skinner, F.K. (2006). Distal gap junctions and active dendrites can tune network dynamics. *Journal of Neurophysiol*, 95, 1669-1682.
- Sherman, A., & Rinzel, J. (1992). Rhythmogenic effects of weak electrotonic coupling in neuronal models. *Proceedings of the National Academy of Science USA*, 89, 2471-2474.
- Skinner, F.K., Zhang, L., Perez Velazquez, J., & Carlen, P. (1999). Bursting in inhibitory interneuronal networks: A role for gap-junctional coupling. *Journal of Neurophysiology*, 81, 1274-1283.

- Söhl, G., Maxeiner, S., & Willecke, L. (2005). Expression and functions of neuronal gap junctions. *Nature Reviews Neuroscience*, 6, 191-200.
- Stiefel, K.M., Gutkin, B.S., & Sejnowski, T.J. (2009). The effects of cholinergic neuromodulation on neuronal phase-response curves of modeled cortical neurons. *Journal of Computational Neuroscience*, 26(2), 289-301.
- Traub, R.D., Schmitz, D., Jefferys, J.G.R., & Draguhn, A. (1999). High-frequency population oscillations are predicted to occur in hippocampal pyramidal neuronal networks interconnected by axoaxonal gap junctions. *Neuroscience*, 92, 407-426.
- Vogel, R., & Weingart, R. (2002). The electrophysiology of gap junctions and gap junction channels and their mathematical modelling. *Biology of the Cell*, 94, 501-510.
- Zahid, T., & Skinner, F.K. (2009). Predicting synchronous and asynchronous network groupings of hippocampal interneurons coupled with dendritic gap junctions. *Brain Research*, 1262, 115-129.

Figure Captions

Figure 1. Bistable activity in a pair of electrically coupled LIF cells. $I=1.2$, $\beta=0.2$, $g_{gap}=0.2$. Black solid curves and grey dashed curves represent the membrane potentials of the two cells. Different initial conditions lead to different phase-locked states: (a) synchrony, and (b) anti-phase.

Figure 2. Membrane potential (v_{LC}), iPRC (Z), and G -functions for LIF cell-pair with weak electrical coupling. (a) $I=1.15$, $\beta=0.1$, (b) $I=1.5$, $\beta=0.1$. In G -function panels, black solid lines are the full G -functions, and the filled circles (open circles) represent stable (unstable) phase-locked states. The dashed grey lines are the portion of the G -function accounting for the effects of the spike, which always tend to synchronize activity of LIF cells. The solid grey lines are the portion of the G -function accounting for subthreshold activity (obtained by setting $\beta=0$), which always tend to desynchronize the activity of LIF cells.

Figure 3. Bifurcation Diagram for LIF cell-pair with weak electrical coupling, $\beta=0.1$. Solid and dashed lines indicate stable and unstable phase-locked states respectively. I^* is the critical value of I at which anti-phase activity ($\phi/T=0.5$) changes stability. For $I > I^*$, only the synchronous activity (S) is stable; for $1 < I < I^*$, both the synchronous (S) and anti-phase (AP) states are stable. (I^* decreases as β increases).

Figure 4. Two-parameter (β vs I) bifurcation diagram for the LIF cell-pair connected by weak electrical coupling. The dashed curve plots the critical value I^* in relation to β (see equation (eq: βI)). Above the curve, the only stable phase-locked behavior is synchrony (S). Below the curve, the cells can exhibit either stable synchrony (S) or stable anti-phase activity (AP). Note that increased spike strength β and/or increased applied current I promotes synchronous activity.

Figure 5. Membrane potential (v_{LC}), iPRC (Z), and G -functions for QIF cell-pairs with weak electrical coupling. $I=0.1$, $\beta=0.13$. (a) $v_{reset}=-2.85$, $v_{th}=0.15$. Both the synchronous and anti-phase states are stable. (b) $v_{reset}=-1.50$, $v_{th}=1.50$. Only the synchronous state is stable. (c) $v_{reset}=-0.15$, $v_{th}=2.85$. Only the anti-phase state is stable.

Figure 6. Stability of the anti-phase state: Two-parameter (v_{reset} vs $\log_{10}(\text{frequency})$) bifurcation diagram for a QIF cell-pair connected by weak electrical coupling. The solid curves plot the critical values at which the anti-phase state changes stability as determined by equation (eq: G'). (a) $\beta=0$, $v_{th}-v_{reset}=3$, (b) $\beta=0.25$, $v_{th}-v_{reset}=3$.

Figure 7: Three-compartment model voltages, iPRCs and G -functions. *Top row:* one cycle of the voltage at the soma, proximal dendrite (pd) and distal dendrite (dd) locations. Rightmost plot shows two cycles at all three locations (thickest line is the soma voltage and thinnest line is the dd voltage). *Second row:* iPRCs obtained for perturbations at the soma, pd and dd , with the rightmost plot showing all three (thickest line is soma and thinnest is dd). Note the leftward shift of the iPRC with more distal locations. Zero time refers to the spike peak at the soma.

Third row: G -function for electrical coupling at the soma, pd and dd , with the rightmost plot showing all three (thickest line is for soma coupling and thinnest line is for coupling at dd). Somatic coupling predicts stable synchrony (negative slope at zero), and pd and dd coupling predict stable non-zero phase lags (note zero crossing value for negative slopes). *Bottom row:* two-cell simulation for electrical coupling at the dd location. Plots show voltages at soma, pd and dd locations. Note that the phase lag is the same at all three locations and corresponds to about 10 ms, as predicted by the stable phase lag (zero crossing in third plot of above row of G -function). Note that the scale of the vertical axes for all three plots are not the same.

Figure 1

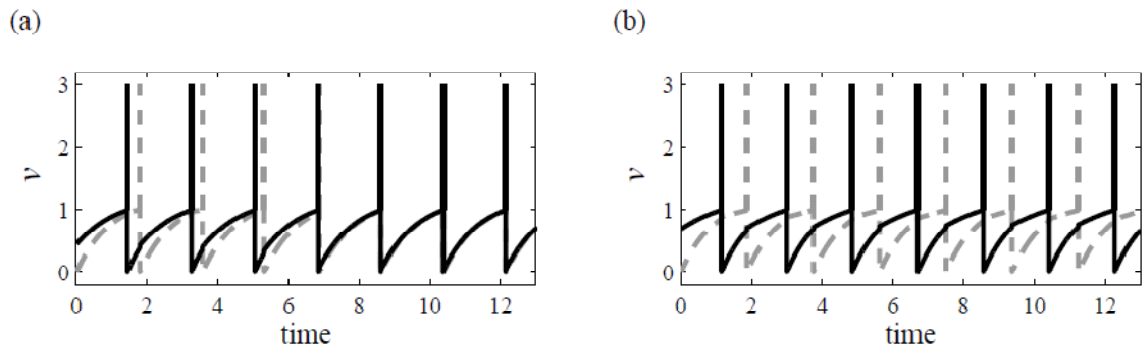


Figure 2

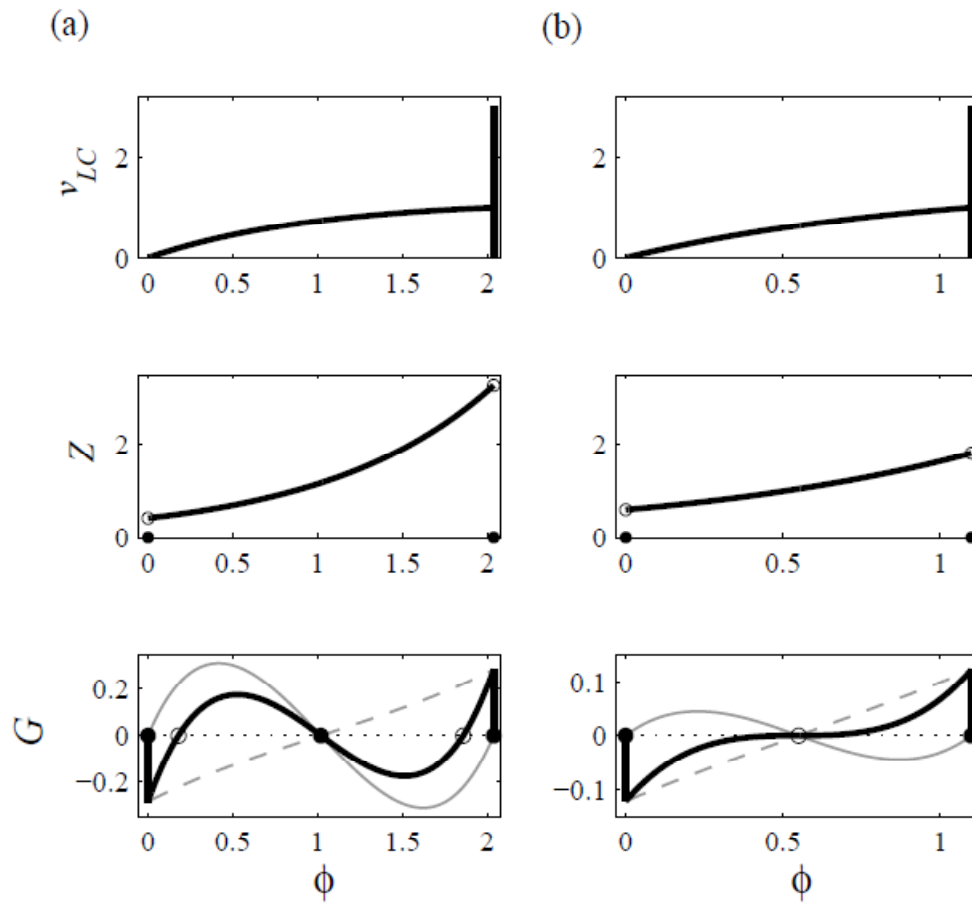


Figure 3

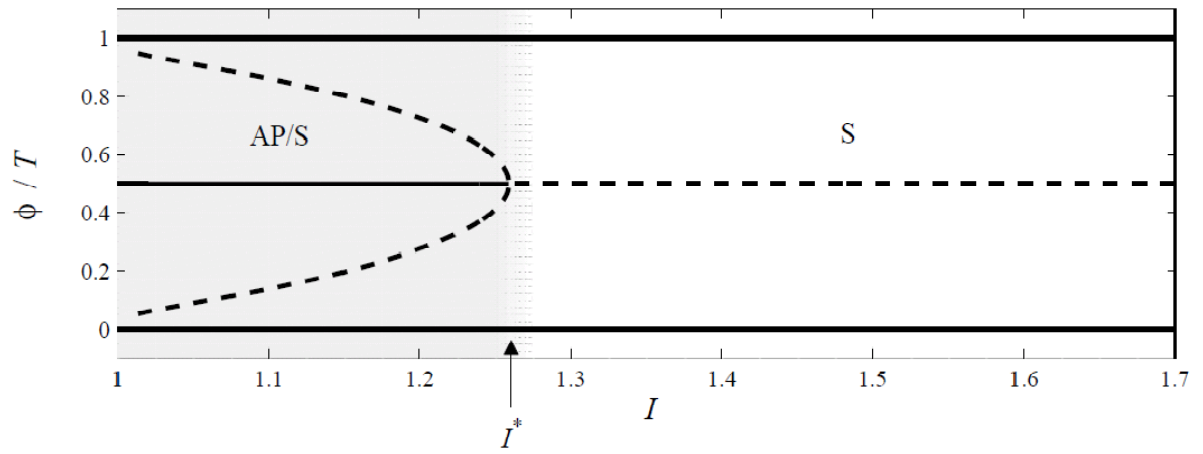


Figure 4

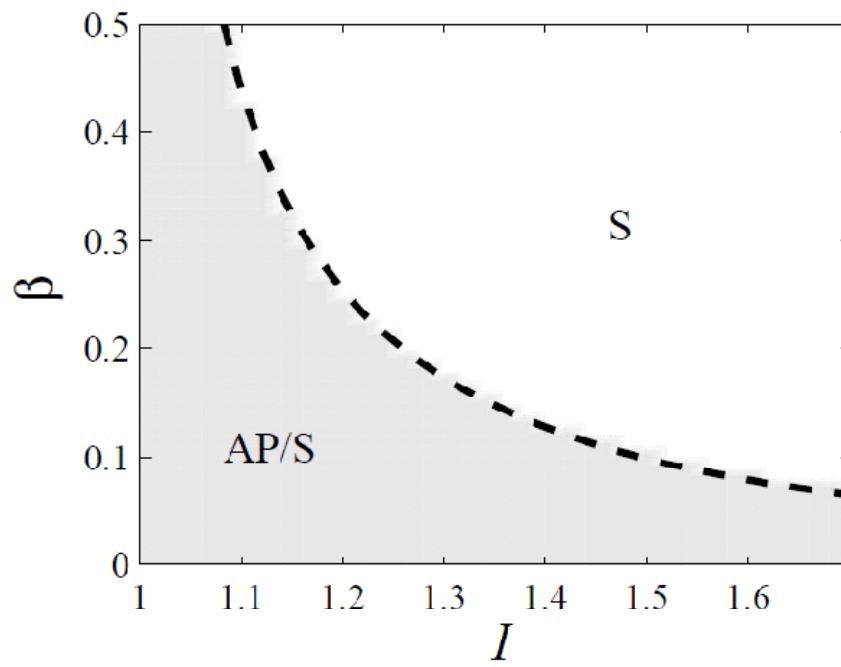


Figure 5

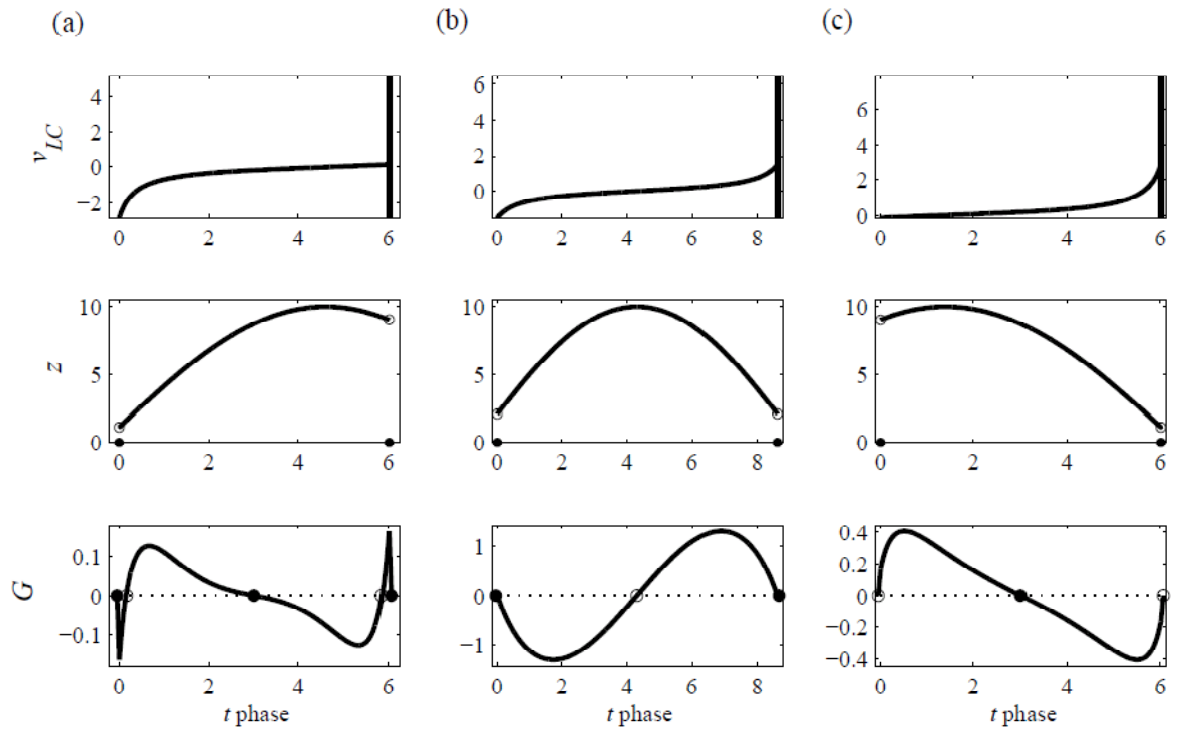


Figure 6

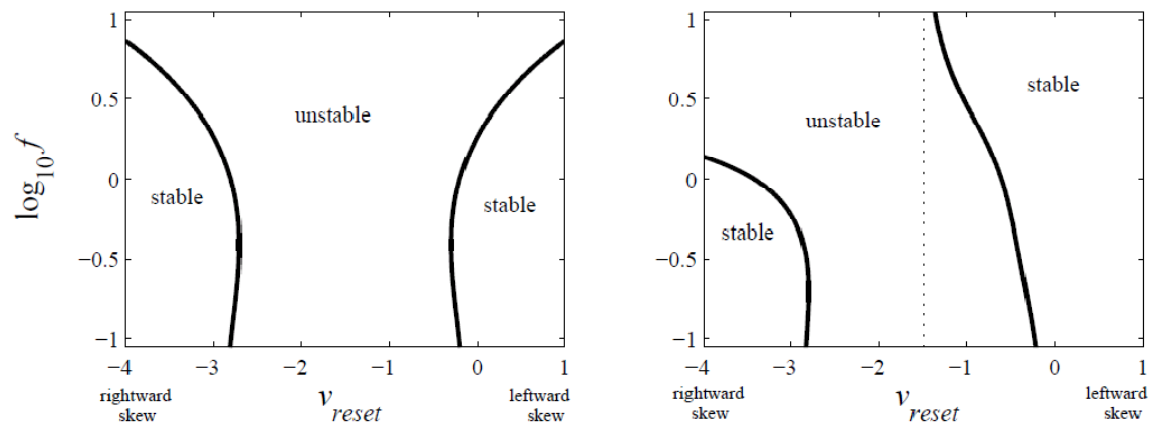


Figure 7

